Sources of Ultra High Energy Cosmic Rays and Neutrinos

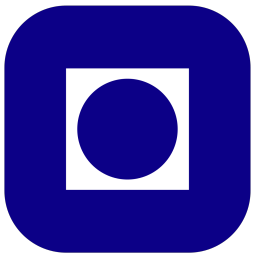

Henrik Døvle Andrews
Norwegian university of Science and Technology

May 4, 2024

Preface

Lorem ipsum dolor sit amet, consectetuer adipiscing elit. Ut purus elit, vestibulum ut, placerat ac, adipiscing vitae, felis. Curabitur dictum gravida mauris. Nam arcu libero, nonummy eget, consectetuer id, vulputate a, magna. Donec vehicula augue eu neque. Pellentesque habitant morbi tristique senectus et netus et malesuada fames ac turpis egestas. Mauris ut leo. Cras viverra metus rhoncus sem. Nulla et lectus vestibulum urna fringilla ultrices. Phasellus eu tellus sit amet tortor gravida placerat. Integer sapien est, iaculis in, pretium quis, viverra ac, nunc. Praesent eget sem vel leo ultrices bibendum. Aenean faucibus. Morbi dolor nulla, malesuada eu, pulvinar at, mollis ac, nulla. Curabitur auctor semper nulla. Donec varius orci eget risus. Duis nibh mi, congue eu, accumsan eleifend, sagittis quis, diam. Duis eget orci sit amet orci dignissim rutrum.

Abstract

Lorem ipsum dolor sit amet, consectetuer adipiscing elit. Ut purus elit, vestibulum ut, placerat ac, adipiscing vitae, felis. Curabitur dictum gravida mauris. Nam arcu libero, nonummy eget, consectetuer id, vulputate a, magna. Donec vehicula augue eu neque. Pellentesque habitant morbi tristique senectus et netus et malesuada fames ac turpis egestas. Mauris ut leo. Cras viverra metus rhoncus sem. Nulla et lectus vestibulum urna fringilla ultrices. Phasellus eu tellus sit amet tortor gravida placerat. Integer sapien est, iaculis in, pretium quis, viverra ac, nunc. Praesent eget sem vel leo ultrices bibendum. Aenean faucibus. Morbi dolor nulla, malesuada eu, pulvinar at, mollis ac, nulla. Curabitur auctor semper nulla. Donec varius orci eget risus. Duis nibh mi, congue eu, accumsan eleifend, sagittis quis, diam. Duis eget orci sit amet orci dignissim rutrum.

Acknowledgments

I would like to thank my supervisor, Professor Foteini Oikonomou, for her guidance and help throughout this project. I would also like to thank my fellow students for their help and support. Balasubramaniam et al. 2021

Contents

List of Figures

List of Tables

1 Introduction

1. The motivation for looking for UHECRs and Neutrinos
2. What multimessenger astronomy can give us
3. The difficulty of knowing the sources of multimessengers
4. The possible source population
5. Outline

2 The ever-expanding Universe

To investigate sources very far away from an observer it is important to understand the influence this distance has on the desired observables. Therefore, in astrophysics and astronomy in general there are distances created to take into account the effects of an expanding Universe. This chapter draws heavily from Hogg 2000.

2.1 Cosmological parameters

A reasonable place to start is with the Hubble constant H_0. This parameter sets the recession speed of a point at proper distance d and the current position via the relation $v = H_0 d$. The subscript 0 refers to the present epoch signifying that H_0 is not static but changes with time. The precise value of H_0 is quite debated, so it's commonly expressed in a parameterised form,

$$H_0 = 100 \frac{\text{km}}{\text{s}} \frac{1}{\text{Mpc}} h.$$

The parameter h is a dimensionless number that according to current knowledge can take the value between 0.5 to 0.8 reflecting the range of answers collected from recent work.

Beyond its basic definition, H_0 also allows for the derivation of two significant cosmic scales:

Hubble Time (t_H) : Defined as the inverse of H_0, t_H provides an estimate of the age of the Universe. It sets a scale for the time since the Big Bang, assuming the Universe has been expanding at a constant rate. The equation $t_H = 1/H_0 \approx 14$ Billion years offers a way to approximate this expansion timescale.

Hubble Distance (D_H) : This is a measure of the distance. Calculated as $D_H = c/H_0 \approx 4.4$ Gly, where c is the speed of light, it represents a critical boundary in observational cosmology.

2.2 Shape of the Universe

The shape and expansion of the Universe are central themes in cosmology, but to model such one needs to define the structure of the Universe and its contents. In this report and many articles, the Universe is often explored through the lens of the flat Lambda Cold Dark Matter (ΛCDM) model. This model, widely accepted in contemporary cosmology, provides a framework for understanding the Universe's composition and its expansion dynamics by assuming as the name suggests no curvature and cold dark matter. In the ΛCDM model, two key parameters are important: the mass density of the Universe, ρ_0, and the cosmological constant, Λ. These parameters, which evolve, are a part of defining the metric tensor in general relativity, thereby allowing us to model the curvature of the Universe based on its initial conditions. These parameters are often expressed as dimensionless variables:

$$\Omega_m = \frac{8\pi G \rho_0}{3H_0^2}$$

$$\Omega_\Lambda = \frac{\Lambda c^2}{3H_0^2}$$

Here, Ω_m represents the matter density parameter, encompassing both ordinary (baryonic) matter and dark matter. Ω_Λ, on the other hand, corresponds to the density parameter associated with the cosmological constant, which is often interpreted as dark energy.

In general, one has a third density parameter Ω_k which defines the curvature of space-time and the relationship between these parameters is expressed as:

$$\Omega_m + \Omega_\Lambda + \Omega_k = 1$$

In a flat Universe, one has $\Omega_k = 0$ and the Universe is dominated by dark energy and dark matter. The model used in this report and the papers used in the following chapters is the flat ΛCDM model where the parameters take the values of $\Omega_\Lambda = 0.7$ and $\Omega_m = 0.3$. These values align with current observational data.

2.3 Redshift

Redshift is defined as the fractional Doppler shift of emitting light. The Doppler effect is a known effect on different observables in the Universe where the relative motion of sources to observers will impact the observable. The redshift is quantified for a light source as

$$z = \frac{\nu_e}{\nu_o} - 1 = \frac{\lambda_o}{\lambda_e} - 1 \tag{1}$$

Here o refers to the observed quantity and e the emitted. Due to the expansion of the Universe the light emitted from a distant source will be increasingly redshifted the further away it is. In these scenarios the redshift serves as a distance measure, allowing us to deduce distances to faraway objects.

2.4 Comoving distance

Comoving distance is an important concept in cosmography, acting as a standard unit for various distance measurements in the Universe. This distance, often termed the line-of-sight distance for an observer on Earth, remains constant even as objects expand with the Hubble flow. To calculate the total comoving distance (D_c) to an object, one integrates the differential comoving distances (δD_c) along the line of sight, starting from redshift $z = 0$ to the object. This integration necessitates consideration of the Universe's parametric composition and the δD_c is expressed as

$$\delta D_c = \frac{D_H}{E(z)} dz, \tag{2}$$

where the function $E(z)$ is defined as

$$E(z) = \sqrt{\Omega_m (z+1)^3 + \Omega_k (1+z)^2 + \Omega_\Lambda}. \tag{3}$$

Here, $E(z)$ incorporates the density parameters previously discussed and the redshift z. It also relates to the Hubble constant observed by a hypothetical observer at redshift z, expressed as $H(z) = H_0 E(z)$.

One then calculates the comoving distance D_c from

$$D_c = D_H \int_0^z \frac{dz}{E(z)} \tag{4}$$

In addition to the line of sight, one can define the transverse comoving distance D_m. This distance relates two points in the night sky at the same redshift separated by an angle $d\theta$. The actual distance between them $d\theta D_m$ will then vary depending on the curvature of the Universe. This relationship is summarized in

the following equation which accounts for different geometries,

$$D_m = \begin{cases} D_h \frac{1}{\sqrt{\Omega_k}} sinh(\frac{\sqrt{\Omega_k} D_c}{D_H}) & \text{if } \Omega_k > 0 \\ D_c & \text{if } \Omega_k = 0 \\ D_h \frac{1}{\sqrt{|\Omega_k|}} sin(\frac{\sqrt{|\Omega_k|} D_c}{D_H}) & \text{if } \Omega_k < 0 \end{cases}$$

The different cases correspond to hyperbolic, flat, and spherical geometry respectively. The true nature of the Universe is still unknown, but recent observations indicate a flat Universe.

2.5 Luminosity distance

The luminosity distance D_l is defined through the relation between the bolometric flux F of a source and its bolometric luminosity L. Bolometric flux is the energy received per unit of time per unit area without any obscuration, while bolometric luminosity is the total energy emitted per unit of time. The luminosity distance is defined as

$$D_l = \sqrt{\frac{L}{4\pi F}} \tag{5}$$

It is related to the transverse comoving distance via

$$D_l = (1+z) D_m. \tag{6}$$

If one wants to calculate the spectral flux/ differential flux one needs to take into account a correction. This correction comes from the fact that one is viewing a redshifted object. The object is emitting in a different band than observed. The spectrum of the differential flux F_ν is related to the spectral luminosity via

$$F_\nu = (1+z) \frac{L_{(1+z)\nu}}{L_\nu} \frac{L_\nu}{4\pi D_l^2}. \tag{7}$$

All these equations listed help include the effects of an expanding Universe when astronomers study distant objects and their properties.

3 High Energy Particles

1. Introduction to high energy particles, cosmic rays, and neutrinos. The standard model.
2. The acceleration mechanisms of cosmic rays and neutrinos., derive the power of a particle undergoing first order Fermi acceleration.
   (a) The Hillas criterion
   (b) Derive the power of a particle undergoing first order Fermi acceleration.
   (c) Timescales for acceleration
3. Talk about the nature of Cosmic rays
   (a) The composition of cosmic rays
   (b) Energy loss mechanisms of cosmic rays
      i. Photopion production
      ii. Synchrotron radiation
      iii. GZK cutoff
      iv. Pair production
      v. local volume limit due to these losses
   (c) Detection
      i. Detectors and retracing
      ii. Emissivity of local volume
      iii. Spectrum
4. Neutrinoes
   (a) Production
   (b) Flavour mixing
   (c) Energy loss mechanism
   (d) Detection
      i. detectors and difficultu of detection
      ii. retracing
      iii. Emissivity of local volume?
      iv. Spectrum

In this section one will define and discuss the nature of high energy particles such as high energy cosmic rays(UHECRS) and neutrinos.

3.1 Acceleration of high energy particles

Acceleration of high energy particles is still a complicated problem in astrophysics and there are still many open questions. The main ways of acceleration are through shocks, magnetic reconnection, and one-shot acceleration, and one will go through to varying degree these methods in this section.

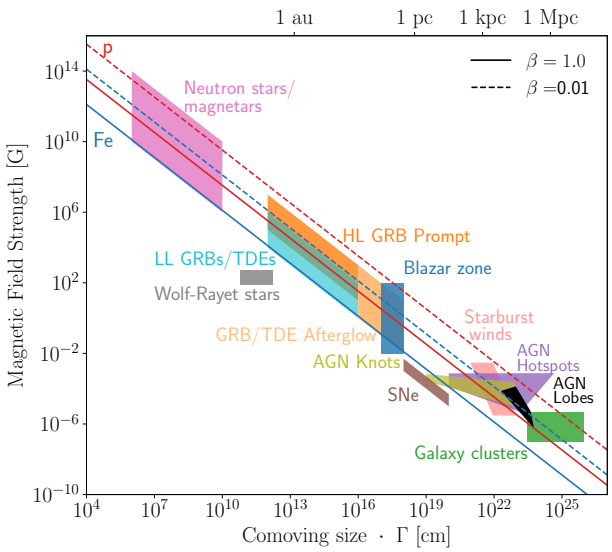

Figure 1: Hillas criterion for proton (blue line) and iron (red line) accelerated up to $10^{20}eV$ and $10^{21}eV$ respectively

3.1.1 The Hillas criterion

Before one delves into macroscopic acceleration models one can start with a bigger picture. By arguing that the acceleration, whatever it may be, needs to be of a certain strength and that the particle being accelerated needs to stay confined within the accelerating region for long enough one can create an upper band on the maximum energy reach by charged particle. This simple but powerful criterion is called the Hillas criterion introduced in Hillas 1984, and is a way of estimating the maximum energy a particle can reach in a given source for a given uniform magnetic field.

For relativistic particles with charge Z and energy ϵ in a magnetic field of strength B one can define the Larmor radius

$$R_L = \frac{\epsilon}{ZB} \tag{8}$$

By arguing that the confinement of a particle to an accelerating region is the same as setting the Larmor radius equal to the size of the source, one can easily derive the maximum achievable energy for a particle as follows;

$$\epsilon_{max} = ZBR \tag{9}$$

Via this method, one can estimate the potential candidates that can produce the observed high-energy particles. The criterion works as an upper boundary of acceleration sources since it does not account for energy loss in the acceleration process or any type of interaction that one could expect to be in turbulent environments. In figure 1 one can see the different candidates for the acceleration of two different ions, protons, and iron. One of the candidates is the AGN, which is the focus of this paper.

3.1.2 Macroscopic Acceleration mechanisms

In order to accelerate particles to high energies, one needs to have a mechanism that can transfer energy to the particles. This usually happens through electromagnetic fields, and there are several ways this is thought to happen.

One-shot acceleration: The simplest yet still a powerful way of accelerating particles is through what is called one-shot acceleration. In the presence of an ordered electricmagnetic fields, one can continuously accelerate charged particles which will follow the field lines. This can be induced from a rotating magnetic field or a straight electric field, all which create and electromagnetic force on a hypothetical charged particle. This could be the feature of some astrophysical objects such as neutron stars and black holes, usually in a quite close proximity to the object in question.

Second order Fermi acceleration/Diffusive acceleration In regions where one has high variability in the magnetic field strength, one can accelerate particles via scattering. The idea is that charged particles scatter on what can be seen as magnetic clouds and gain energy in the process due to the speed of the clouds. This mechanism is dubbed second order fermi acceleration due to the average energy gain of a particle being proportional to $(\frac{v}{c})^2$. Here v is the speed of the cloud and c is the speed of the particle. This is a slow process due to the proportionality to v^2, but as mentioned in C. Dermer 2001 can be a viable way of accelerating particles which already have a high energy. In modern times the magnetic mirrors that particles scatter on are thought to be plasma waves. The idea is that particles occupy a background magnetic field B_0 with a superimposed fluctuating electromagnetic field which arrise due to cold-plasma waves. The full formalism is described in C. D. Dermer and Menon 2009 at page 361. In trying to shorten the explination on only focuses on the resulting energy gain. The mean rate of change of the momentum of a particle is given as

$$\left\langle \frac{dp}{dt} \right\rangle = \frac{1}{p^2} \frac{\partial}{\partial p} \left[p^2 D(p) \right] \tag{10}$$

where the real challenge lies in determining the diffusion coefficent $D(p)$ which is a function of the particle momentum and pitch angle. One will follow the approach found in O'Sullivan, Reville, and Taylor 2009 in which one only considers alfvén waves which take a one-dimensional power spectrum $W(k) \propto k^{-q}$, where q is the spectral index and the total internal energy of the waves is given as $\frac{\delta B^2}{8\pi} = \int_{k_{min}}^{k_{max}} W(k) dk$.

As given in O'Sullivan, Reville, and Taylor 2009 the diffusion coefficient with current wave spectrum can be given as

$$D(p) = \beta_a^2 \frac{\delta B^2}{B_0^2} \left(\frac{r_g}{\lambda_{max}} \right)^{q-1} \frac{p^2 c^2}{r_g c} \tag{11}$$

where $\beta_a = \frac{B}{\sqrt{4\pi n_p m_p c}}$ is the alfvén speed, $r_g = \frac{pc}{ZeB}$ is the gyroradius of the particle, and λ_{max} is the maximum wavelength of the waves, which will be specified when necessary, but if one is following O'Sullivan, Reville, and Taylor 2009 takes the value of $0.1R$, i.e. a magnitude lower than the radius of the emitting region.

Form here one can estimate the acceleration timescale of a particle in a given region. The timescale is given as

$$t_{acc} = \frac{p^2}{D(p)} \tag{12}$$

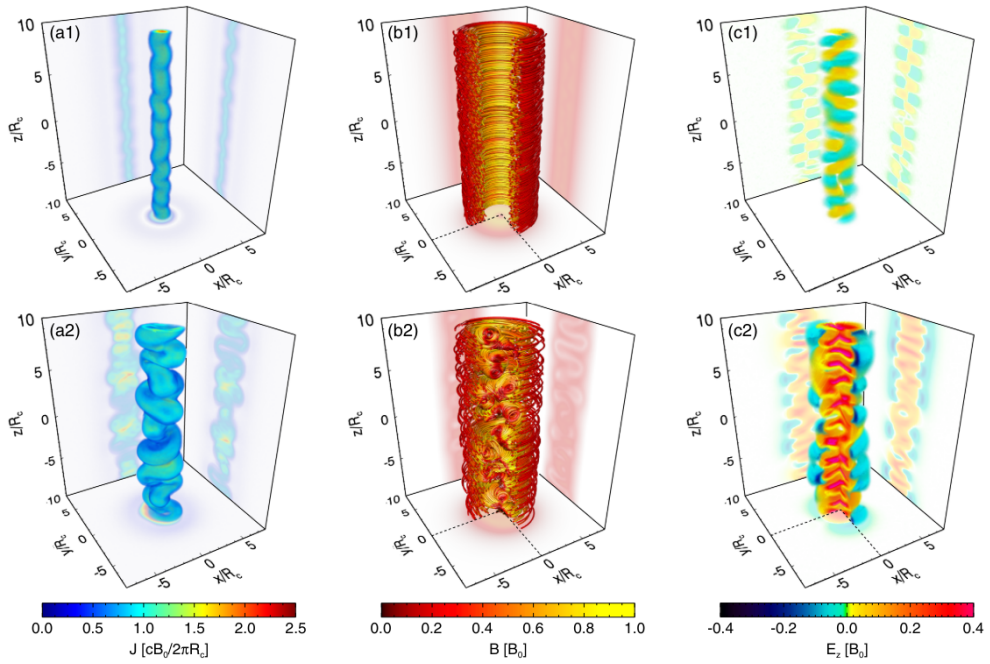

Figure 2: Simulations from Alves, Zrake, and Fiuza 2018 showing the evolution of kink instability in a jet. The upper panels shows the before the KI instability has been amplified, and the lower panel shows the jet after the instability has been amplified. From left to right the panels show, Current density, magnetic field lines, and axial electric field.

First order Fermi acceleration In regions where one has strong shock fronts, one can accelerate particles to high energies. These environments can be found several places where the interstellar medium is interacting with a powerful source of energy. One of the most famous examples of this is the supernova remnant where one sees a powerful shock front as a result of a supernova explosion. The first-order Fermi acceleration happens when particles traverse these strong shock fronts, and when a particle moves through the shock it gains energy proportional to $\frac{v}{c}$. In addition to this, there is a probability that the particle will stay in the accelerating region and experience several accelerations.

In C. Dermer 2001 they can derive the relative power of a particle undergoing first-order Fermi acceleration in a relativistic shock, and it is given as

$$\dot{p} = \frac{2p}{t_u} = \frac{2cqB\Gamma}{mc^2} \tag{13}$$

where t_u is the time in the upstream frame, p is the momentum of the particle, c is the speed of light, q is the charge of the particle, B is the magnetic field strength, Γ is the Lorentz factor of the shock, and m is the mass of the particle.

KI instabilities in jets Another method of acceleration which really is diffusive one shot acceleration related to AGN jets is acceleration via the kink instability in jets. The idea of kink instability leading to acceleration is found in Alves, Zrake, and Fiuza 2018. Kink instability is a hydrodynamic instability that arises in jets when the magnetic field is not aligned with the jet. If a perturbation is introduced to the jet, the resulting force on the jet structure will magnify the perturbation. This will lead the jet to a much more complicated structure, and twist the magnetic field lines. See figure 2 for an illustration. The paper argues that a highly tangled magnetic field and a large scale inductive electric field which is found throughout the kink-unstable region will lead to rapid energization of particles.

3.2 UHECRs

UHECRs are charged particles that are bombarding the Earth with energy exceeding 1 exaelectronvolt (10^{18} eV) according to Alves Batista et al. 2019. The origin of these particles is still a mystery but due to their high energies, they are thought to be extragalactic in origin. The composition of UHECRs ranges from protons to heavier nuclei such as helium or iron, and when these particles interact with the atmosphere they produce a shower of secondary particles. The air showers could also give extra information such as direction, but due to the nature of UHECRs, the location of their source is difficult to pinpoint. This is because UHECRs are charged particles and therefore are deflected by the magnetic fields they encounter.

3.2.1 Production and Energy loss

The requirements to produce a UHECR are a charged particle and a powerful accelerator. But in order to model them sufficiently one needs to take into account their journey to the Earth. Both during the acceleration and during the journey to Earth, the UHECRs will lose energy. The important parameters for this energy loss are its composition and its environment. In addition, as mentioned before, the interstellar magnetic field will also deflect the particles and therefore the direction of the particle will be changed. These effects are important parameters since they limit the distance a particle can travel before it loses too much energy, and therefore limits the local volume in which high energy cosmic rays can be produced. Here I will briefly discuss the different energy loss mechanisms.

4 Probing extra galactic sources

In this section one will outline some different methods and observables used to probe extra galactic sources as potential candidates for the origin of the UHECRs and/or neutrinos. The goal is to constrain our list of candidates by applying known effects and theoretical models to observed data, and to discuss the implications of these constraints. In brief, one will be discussing the energy budget of our sources, the anisotropy of the UHECRs and neutrinos, and a comprehensive time-scale analysis of the sources. In order to do so several key pieces of information is required, which will be discussed in the following sections.

4.1 Density and anisotropy

Due to the non-observation of any dipole moment in the distribution of extra-galactic UHECRs, and neutrinos as discussed in section 3 one can put strict limits on the density of sources. In collaboration 2013 they quote a density larger than $(0.06-5)10^{-4}\mathrm{Mpc}^{-3}$ at a 95% confidence level. This density although not exceedingly large would still damper the idea of singular but powerful sources.

To calculate the density of sources in the Universe there are several methods. The most common method is to use the luminosity function of the sources in question. The luminosity function is a function that describes the number of sources per unit volume and luminosity. Typically, the focus is on the differential luminosity function, which is defined as

$$\frac{d\Psi(L,z)}{dL} = \frac{d^2N(L,V_c(z))}{dLdV_c(z)}. \tag{14}$$

One also can change the differential of the comoving volume into a term only depending on the redshift assuming the source population is isotropic and by multiplying with the differential comoving volume element. This transformation goes as follows,

$$\frac{d^2N(L,V_c(z))}{dLdV_c(z)}\frac{dV_c(z)}{dz} = \frac{N(L,z)}{dLdz}. \tag{15}$$

To effectively determine the LF, it's typical to divided it into two distinct components: a local term and a time evolution term. This approach involves taking the local luminosity function, calculated at a redshift $z = 0$, and then scaling it with a function that accounts for the change in redshift. The exact form of the total LF varies based on the source object, but it generally falls into two categories derived from the method of incorporating the growth term into the local LF. These methods are selected based on which best represents the observed evolution.

The two distinctions are the Pure Density Evolution (PDE) and the Pure Luminosity Evolution (PLE). The PDE model modifies the local density function to reflect changes over time, while the PLE model adjusts the local luminosity. The evolution is better represented by their equations and is given as

$$\frac{d\Psi(L,z)}{d(L)} = \begin{cases} \frac{d\Psi(L/e(z),z=0)}{d(L)} & (PLE) \\ \frac{d\Psi(L,z=0)}{d(L)}e(z) & (PDE) \end{cases}. \tag{16}$$

For some sources which lack obersvational data it can be difficult to estimate a full luminosity function. Due to the lack of observation or a big bias in the catalogue selection difference sources are not constrained enough and therefor one must rely on simpler estimates to get the order of magnitude. One such method given that the lifetime of a sources is know is via simple probability. One wished to estimate their required density to produce the observed amount of sources, or in the worst case one source given its average lifetime.

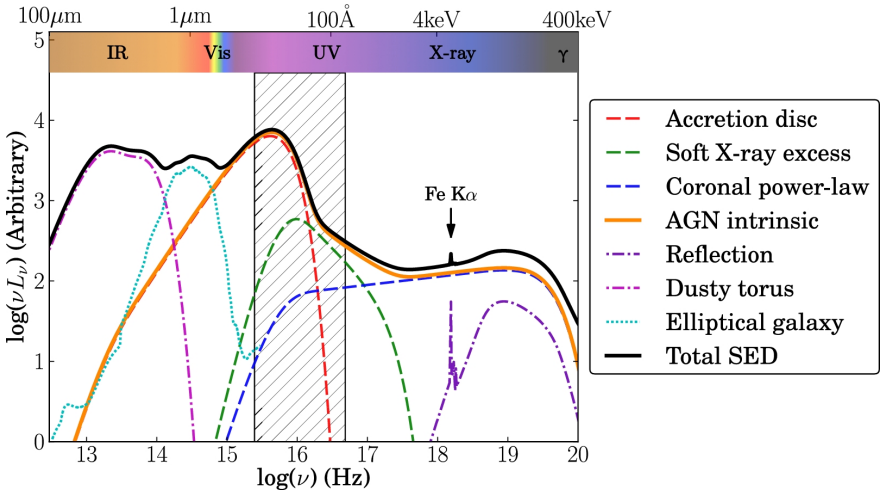

Figure 3: The spectral energy distribution of a typical AGN viewed without interference from the jet. The different components of the AGN are visible in the plot. Image taken from Collinson et al. 2016

This will in most cases serve as a lower limit, and give us a starting point for further analysis.

in order to do so, one defines the probability of seeing a single source that has a lifetime t_l up to a horizon t as

$$p = \frac{t_l}{t}. \tag{17}$$

The horizon is the redshift at which one stops finding appreciable number of your source. The required density such that one observes 1 source at present time can then be estimated as

$$n = \frac{1}{pV} \tag{18}$$

The calculation is crude, but very solid, and allows us to make lower limit estimates on sources where the Luminosity function is not defined.

4.2 SED broad band analysis

The spectral shape of emitting galaxies and galaxy cores tell us a lot about the underlying dynamics, and with this information one can start to peel away the complex layers. The spectral energy distribution (SED) of a source is a plot of the energy emitted by the source as a function of frequency. In figure 3 on can see the typical SED of an AGN in which the jet components, that is to say the synchrotron and inverse Compton components, are not dominant. The different components of the AGN are visible in the plot, and understanding how different components are created and contributing to the nearby enviroment will give us a better understanding of what observables one might expect from sources such as these. The main idea of these areas being good probes for UHECRs and Neutrinos is that the relativistic electrons are thought to be accompanied by relativistic protons. The true composition of the relevant areas are not known and still is a big question in this realm of research.

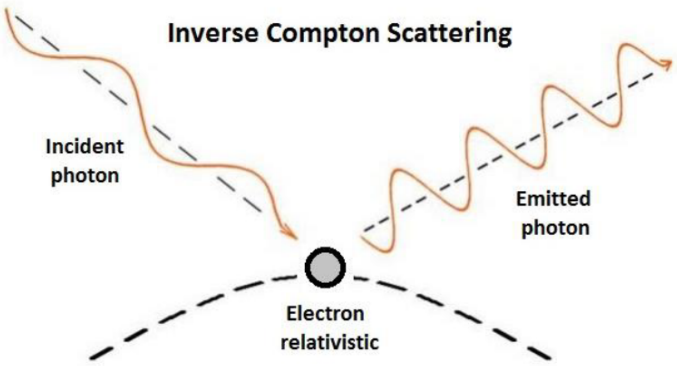

Figure 4: The inverse Compton scattering process. The process is the scattering of a low energy photon by a relativistic electron. The scattered photon will have a higher energy than the original photon. Image taken from Bennun 2020

4.2.1 X-ray energy budget

The X-ray energy budget of especially Active galactic nuclei is often used as a probe for UHECRs and neutrino emissivity. This makes the X-ray Luminosity of AGN an interesting parameter that warrant further analysis. In this sense the X-ray luminsoity is often used a proxy for the total energy budget of escaping particles, but a true relation between the two is not known. The X-ray luminosity of an AGN usually has two sources of emission, the corona, and IC scattering of the synchrotron radiation in the jets. In both cases the main mechanism is thought to be Inverse Compton scattering and for that one requires relativistic electrons. Requiring relativistic electrons is a good indicator that there might be relativistic protons present as well, and following that logic one can start to estimate the energy budget of the protons.

4.2.2 Radio luminosity

4.2.3 Photon fields around AGN

In order to determine the photon fields we follow Ghisellini and Tavecchio 2009 which describe the photon fields surrounding a Blazar. The photon fields separates into different contribution from the different regions of a classic AGN as discussed in section ... The different regions are the accretion disk, the broad line region, the torus and the x-ray corona.

Accretion disk: The photon field emerging from an accretion disk if calculated by assuming a black body spectrum at each ring of an Shakura-Sunyaev disk and summing up its contributions. The temperature of each ring in the disk is given by

$$T(R) = \left(\frac{3R_S L_d}{16\pi R^3 \eta \sigma_{\mathrm{SB}}} \left(1 - \left(\frac{3R_S}{R} \right)^{\frac{1}{2}} \right) \right)^{\frac{1}{4}} \tag{19}$$

Each ring of the accretion disk is assumed to be at the same temperature and emitting as a black-body spectrum. By using this temperature one can use the black body spectrum of an object with temperature T to find the intensity:

$$I(\nu) = \frac{2h\nu^3}{c^2}\left(\frac{1}{\exp\left(\frac{h\nu}{k_B T}\right) - 1}\right) \tag{20}$$

By integrating the intesity over all annuli of the disk one can find the total flux of the disk and from there the total energy density of the disk per frequency. This then needs to be scaled to incorporate the location of our emitting region which sits at a distance R from the accretion disk.

The resulting spectral energy density is then given by

$$U_d(\nu) = \frac{2\pi}{c}\int_{\mu_d}^{1} I(\nu)d\mu \tag{21}$$

where μ_d is the cosine of the angle between the location on the disk and the normal of the disk with respect to and observer.

X-ray corona: The photon field from the x-ray corona is assumed to be a power law spectrum with a cut off at high energies. Its total energy emitted is related to the disk Luminosity by the equation $L_{cor} = fL_d$ where f is the fraction of the disk luminosity that is emitted by the corona. The spectral energy density of the corona is then given by

$$U_{cor}(\nu) = D(R)\left(\frac{\nu}{\nu_0}\right)^{-\alpha}\exp\left(-\frac{\nu}{\nu_{cut}}\right) \tag{22}$$

The factor $D(R)$ is a scaling factor that incorporates the position of the observer in similar fashion to the disk. The integral of the spectral energy density over all frequencies should equate to the total energy density in x-ray at the location of the emitting region.

The energy density of x-ray around the central engine is given by a

$$\mathrm{UX}(R) = \frac{f_X L_d \Gamma^2}{\pi (R_X)^2 c}\left(1 - \mu_X - \beta(1-\mu_X^2) + \frac{\beta^2(1-\mu_X^3)}{3}\right) \tag{23}$$

where

$$\mu_X = \left(1 + \frac{R_X^2}{R^2}\right)^{-0.5}.$$

Here f_X is the fraction of the disk luminosity that is emitted by the x-ray corona, L_d is the disk luminosity, Γ is the lorentz factor of the jet, R_X is the size of the x-ray corona, c is the speed of light, β is the velocity of the observer in units of the speed of light. In short the x-ray energy density stays constant until the observer is further away where it will decrease as $1/R^2$ which is to be expected.

Broad line region: The broad band field is assumed to be emitting a black body spectrum as in 20 which peaks at the Lyman-alpha line. The Lyman-alpha line is a spectral line of hydrogen when the atomic electron transitions from the $n = 2$ to the $n = 1$ orbital corresponding to a frequency of $\nu_\alpha = 2.47 \times 10^{15}$ Hz. Similarly to the x-ray corona the spectral energy density is scaled to the region of interest and the total energy density is given by:

$$\mathrm{UBLR}(R) = \begin{cases} \frac{f_{\mathrm{BLR}} L_d \Gamma^2}{\pi R_{\mathrm{BLR}}^2 c} & \text{if } R \leq R_{\mathrm{BLR}}, \\ \frac{f_{\mathrm{BLR}} L_d \Gamma^2}{\pi R_{\mathrm{BLR}}^2 c \beta 3} \left[2(1-\beta\mu_{\mathrm{IR1}})^3 - (1-\beta\mu_{\mathrm{IR2}})^3 - (1-\beta)^3\right] & \text{if } R \geq 3R_{\mathrm{BLR}}, \\ aR^b & \text{otherwise,} \end{cases} \tag{24}$$

where

$$\mu_{\mathrm{IR1}} = \left(1 + \frac{R_{\mathrm{BLR}}^2}{R^2}\right)^{-0.5},$$
$$\mu_{\mathrm{IR2}} = \left(1 - \frac{R_{\mathrm{BLR}}^2}{R^2}\right)^{-0.5},$$

Torus: There is also assumed to be a dusty torus around the AGN emitting in infrared. The spectral energy density of the torus is also given by a black body spectrum with the temperature of the tours being set at $T_{\mathrm{IR}} = 370$ K. The total energy density of the torus has the same relations as equation 24 but with the relevant parameters for the torus.

$$\mathrm{UIR}(R) = \begin{cases} \frac{f_{\mathrm{IR}} L_d \Gamma^2}{R_{\mathrm{IR}}^2 c} & \text{if } R \leq R_{\mathrm{IR}}, \end{cases} \tag{25}$$

For illustrative purposes one can see the total spectral energy density in figure 8.

4.3 Magnetic field constraints

4.3.1 Equipartition

The most well know estimate for magnetic field strength in astrophysical sources is throught the equipartition argument. The fact that one observes synchrotron radiation implies that a source of relativistic electrons which have an energy density U_e and that these electrons are in a magnetic field with an energy density U_B. The question that one aims to answer with the equipartition argument is what is the minimum total energy in both relativistic particles and magnetic fields required to produce the observed synchrotron radiation of a given frequency. The toal energy in relativistic particles and magnetic fields of a volume V is given as

$$U_{tot} = U_e + U_B = V(u_p + u_{mag}) \tag{26}$$

Here u_p is the energy density of all relativisitc particle, i.e. electrons, protons and heavyer ions ($Z > 1$). Ions emit very little synchrotron radiation for a given energy E compared to electrons, so little is know about their energy density, therefore it is common to assume

$$u_p = \eta u_e \tag{27}$$

where η is a constant $>$ 1and u_e is the energy density of the relativistic electrons. In order to estimate the energy density of the electrons one assumse their distribuition as a powerlaw $n(E) \propto E^{-\delta}$, and their energy density becomes

$$u_e = K \int_{E_{min}}^{E_{max}} E^{1-\delta} dE \tag{28}$$

In order to move one it is require to know the spectrum of synchrtron radiation for one electron in a particular magnetic field. The derivation is a tedious process, and one will give the results obtained in Wilson, Rohlfs, and Huttemeister 2013 chapter 10.10 and 10.8. The radiated power of an electron peaks strongly around the critical frequency ν_c and one can then write a relation between a frequency ν and energy E as

$$\nu = \frac{3}{2} \frac{eB}{m_e^3 c^5} E^2. \tag{29}$$

This allows for the particle energy density to be written as

$$u_p = K \frac{\eta}{1-2n} \left(\frac{e}{m^3 c^5} \right)^{n-1/2} \left(\nu_{max}^{1/2-n} - \nu_{min}^{1/2-n} \right) B^{n-1/2} = KGB^{n-1/2} \tag{30}$$

by introducing the constant $n = \frac{1}{2}(\delta - 1)$.

The energy density of the magnetic field is given as

$$u_{mag} = \frac{B^2}{8\pi} \tag{31}$$

To move further one wished to eliminate the factor K from our equations, and relate it to observed properties. Wilson, Rohlfs, and Huttemeister 2013 gives the emissivity of a synchrotron source for tangled magnetic fields as

$$\epsilon(\nu) = b(n) K \frac{e^3}{mc^2} \left[\frac{3e}{4\pi m^3 c^5} \right]^n B^{n+1} \nu^{-n} = HKB^{n+1} \nu^{-n}, \tag{32}$$

where $b(n)$ is a function of the spectral index n. The observed flux density of a source with volume V and at distance R is given as

$$S(\nu) = \frac{V}{R^2} \epsilon(\nu) \propto B^{n+1} \nu^{-n} \tag{33}$$

Using this relation one can then write the total energy density while inserting 33 as K in 30 as

$$U_{tot} = \frac{G}{H} R^2 (S_v \nu^n) B^{-3/2} + \frac{VB^2}{8\pi} \tag{34}$$

Given that one has measurments on distance, volume, flux density one can then estimate the magnetic field strength. One then argues that U_{tot} should have a minimum value and one then finds the magnetic field to be

$$B_{eq} = \left(\frac{6\pi G}{H} \frac{R^2}{V} S_\nu \nu^n \right)^{2/7} \tag{35}$$

This relationship between U_B and U_e at this minimum is very near the equipartition value, which is why

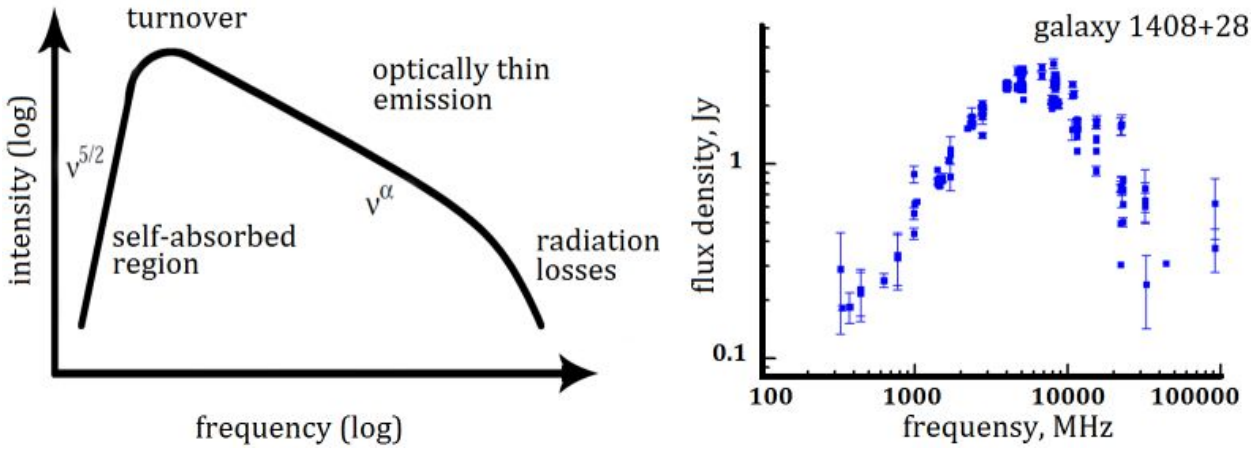

Figure 5: The synchrotron spectrum of a Giga hertz peaked galaxy. Later on one will realise that GHP galaxies and CSO occupy that same niche. Image taken from Group of Active Galactic Nuclei investigation at https://www.sao.ru/hq/giag/gps-en.html

this method is often called as such.

4.3.2 Self synchrotron absorption

The theory of synchrotron self absorption is a tool used previously for estimating magnetic field strength in spherically symmetric synchrotron sources. Synchrotron radiation is the product of charged particles traveling in a magnetic field. The radiation is emitted when the particles are accelerated which happens when an electron is spiraling in an uniform magnetic field. The light is usually highly polarized and is dependent on the electron energy and the magnetic field strength. Moving further along, synchrotron self absorption is the process where the synchrotron radiation is absorbed by the same electrons that produced it, and the effect of this is that any given volume of emitting plasma that radiate synchrotron radiation will have a frequency below which the radiation is absorbed. This frequency is called the turnover frequency, and one aims to show how one can estimate the magnetic field strength in the emitting plasma based on this information. The concept was first introduced by Marscher 1983, but this section relies heaviliy on Hirotani 2005 for the derivation.

Before we begin the derivation it is fitting to understand the spectrum of synchrotron radiation from a plasma. The spectrum is characterized by the peak frequency, also called the turnover frequency ν_m, the peak flux density S_m, and naturally the spectral index α. One referse the reader to image 5 for a simple view of the synchrotron speaktrum in question.

In order to estimate the magnetic field strenght we must assume that it is uniform and that the electron density is also uniform. From here the transfer equation for synchrotron radiation gives in Hirotani 2005 gthe specific intensity as

$$I_\nu = A(\alpha)\nu^{*\frac{5}{2}}[1 - exp(-\alpha_\nu^* x_0^*)] \tag{36}$$

where

$$A(\alpha) = \frac{3}{2}^{-\alpha} \frac{e}{c} \frac{a(\alpha)}{C(\alpha)} \left(\frac{e}{2\pi m_e c}\right)^{-3/2} B^{-1/2} \tag{37}$$

and x_0^* give the thickness of the emitting plasma along the observers line of sight. The coefficients $a(\alpha)$ and $C(\alpha)$ are tabulated values that depend on the spectral index α not to be confused with the absorption coefficient α_ν and any value denoted with an asterix is in the comoving frame.

Imagining an observer at a distance D with angle θ from the blob of plasma(as seen in figure 6), one can define the fractional thickness, which is a Lorentz-invariant quantity, as

$$\frac{x_0^*}{2R^*} = cos(\theta + \xi) = \sqrt{1 - \left[\frac{sin(\theta)}{sin(\theta_d/2)}\right]^2} \tag{38}$$

Determining that $\tau(0) \equiv= \alpha^* 2R^*$ is the optical depth for $\theta = 0$ one can then get the full specific intensity as

$$I_\nu(\theta) = \left(\frac{\delta}{1+z}\right) A(\alpha)\nu^{\frac{5}{2}} \left(1 - exp\left(-\tau(0)\sqrt{1 - \left[\frac{sin(\theta)}{sin(\theta_d/2)}\right]^2}\right)\right) \tag{39}$$

The shape of the blob is assumed to be spherical and we can now integrate the specific intensity over the entire blob to get the total flux density as

$$S_\nu = 2\pi \int_0^{\theta_d/2} I_v(\theta) cos(\theta)\sin(\theta) = \pi sin^2(\frac{\theta_d}{2})(\frac{\delta}{1+z})^{1/2} A\nu^{5/2} \int_0^1 [1 - exp(-\tau(0)\sqrt{1-x^2})]dx \tag{40}$$

where $x \equiv \left[\frac{sin(\theta)}{sin(\theta_d/2)}\right]^2$. Here we insert what we know about the synchrotron spectrum and the turnover frequence ν_m. We derivate the flux density with respect to frequency and set it equal to zero to find the equation that realtes $\tau_\nu(0)$ and α at the turnover frequency. In order to do this one needs to know the relation between the the absorption coefficient and frequency. This is given also in Hirotani 2005 as

$$\alpha_\nu^* = C(\alpha) r_0^2 k_e^* \frac{\nu_0}{\nu^*} (\frac{\nu_B}{\nu^*})^{(-2\alpha+3)/3} \tag{41}$$

where, $\nu_0 \equiv c/r_0$is the electron frequency, $r_0 \equiv e^2/(m_e c^2)$ and $\nu_B \equiv eB/(2\pi m_e c)$ is the cyclotron frequency.

Having the solution for $\tau_\nu(0)$ as a function of α one denotes the solution at the turnover frequency as $\tau_m(0)$. This is a tabulated value and the table from Hirotani 2005 is found in the appendix.

Using this solution one can inversly solve equation 40 for the magnetic field strength B and obtain with the small angle approximation

$$B = 10^{-5} b(\alpha) \left(\frac{S_m}{\text{Jy}}\right)^{-2} \left(\frac{\nu_m}{\text{GHz}}\right)^5 \left(\frac{\theta_d}{mas}\right)^4 \left(\frac{\delta}{1+z}\right) \text{G} \tag{42}$$

where $b(\alpha)$ is a tabulated value as well but arrises from

$$b(\alpha) = 3.98 \times 10^3 \left(\frac{3}{2}\right)^{-2\alpha} \left[\frac{a(\alpha)}{C(\alpha)}\right]^2 \left[\int_0^1 [1 - exp(-\tau(0)\sqrt{1-x^2})]dx\right]^2 \tag{43}$$

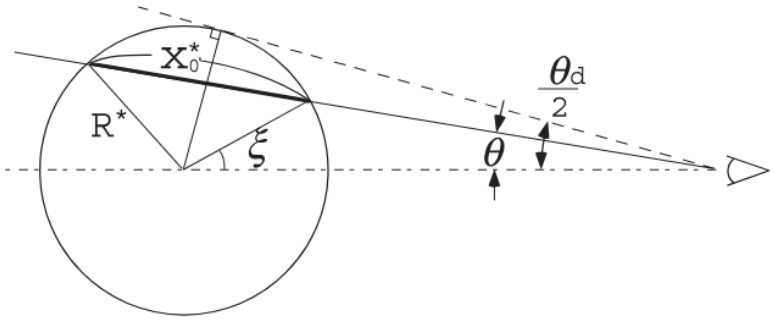

Figure 6: Schematic view of the radiative transfer in a spherical ball of plasma. Image taken from Hirotani 2005

4.3.3 Deviation from SSA and Equipartition

If one calculates the magnetic field using both SSA and Equipartition one expects to not get the exact same results, but given a big discrepancy one cannot assume all the fault lies in only the measurments. In Orienti and Dallacasa 2013 who used SSA and equipartition calculations for a small sample of CSOs, they also found a discrepancy between the two methods. The SSA had a significantly higher value for the magnetic field. This they argue can, and the weight is on can here be induced by a free free absorption effect in the source. Free free absorption is the absorption of radiation by an electron who is in close proximity to an ion. The absorption is a result of the electron being accelerated by the ion and the radiation emitted by the electron is absorbed by the ion. The effect of free-free absorption would shift the spectral peak in SSA to higher frequency and thus give a higher magnetic field strength in our calculations. This would be a good indicator that the source is harbouring ions, which one needs for UHECRs acceleration.

4.4 Time-scales analysis

In order to probe what type of sources could be responsible for the observed UHECRs and neutrinos one can use the relevant time-scales a measure. The timescales of a source will act as an indicator of the dominant processes in the source, and give us an upper boundary for what we could expect of escaping particles. The dominante timescales of a source will be source specific, so further on we will be looking at the timescales of a typical compact AGN. The relevent timescales then are the acceleration timescale, the synchrotron cooling timescale, the dynamical timescale, and the photo-pion cooling timescale.

One starts by determining the acceleration timescale of a proton undergoing first order fermi acceleration, the acceleraiton mechanisms explained in section ... . The acceleration timescale is given by the equation

$$t_{acc} = \frac{\eta\epsilon}{ZeBc} \tag{44}$$

Where η is the efficiency of the acceleration process with the most efficient acceleration harbouring the value $\eta \approx (1-10)$, ϵ is the energy of the particle, Z is the charge of the particle, e is the elementary charge, B is the magnetic field strength and c is the speed of light. Usually the value of η is taken to be 1, which is the most efficient acceleration process.

The dynamical timescale is a limit on the sources size and can be estimated several ways. The sources size is important since in order to accelerate particles the source must also be able to contain particles. If one does not have good measurments on the source size, but have good fluence measurments of an attributing light curve one can estimate the size of the source via the variablility. From the variablility timescale t_{var}

one can estimate the size of the source as

$$R = \frac{c\Gamma t_{var}}{1+z} \tag{45}$$

Another way of estimating the sources size is through telescope measurments. For radio sources one can acheive suffucent accuracy in measurments to estimate the size of the source. If radio if one has the full widht at half maximum of the source one can realte this to the total angular size of a spherical source according to Marscher 1983 as $\theta = \theta_{\mathrm{FWHM}} 1.8$. If one then knows the distance to the source one can get the physical/linear size of the source as

$$D_{\mathrm{size}} = (\theta_{\mathrm{FWHM}} 1.8) \cdot D_A(z) \tag{46}$$

Where $D_A(z)$ is the angular diameter distance to the source at its redshift z.

In the source of AGN there will be an enviroment of magnetic fields and photon fields that will interact with the particles. An important timescale to consider given this enviroment is often the synchrotron cooling timescale. This is the timescale for a particle to lose energy due to synchrotron radiation. One will have both synchrotron losses for proton and for electrons, but since one is concerned about UHECRs one will focus on protons. The synchrotron cooling timescale for protons is given by the equation

$$t_{sync} = \frac{6\pi m_p^4 c^3}{\sigma_T m_e^2 B^2 E}. \tag{47}$$

Here, m_p is the proton mass, m_e is the electron mass, σ_T is the Thompson cross-section, B is the magnetic field strength, E is the energy of the particle and c is the speed of light.

The last timescale used in this analysis is the pion production timescale. Due to the photon fields a proton will inhabit while accelerating, one needs to consider the pion production timescale. This is the timescale for a proton to interact with a photon and produce a pion. The equation is given by

$$t_{pr}^{-1}(\varepsilon_p) = \frac{c}{2\gamma_p^2} \int_{\varepsilon_{th}}^{\infty} d\varepsilon \sigma_{pr}(\varepsilon) k_p(\varepsilon) \int_{\varepsilon/2\gamma_p}^{\infty} d\varepsilon' \varepsilon'^{-2} \frac{dn}{d\varepsilon'} \tag{48}$$

where ε_p is the energy of the proton, γ_p is the lorentz factor of the proton, ε_{th} is the threshold energy for the interaction, σ_{pr} is the cross-section for the interaction, k_p is the photon field, and $dn/d\varepsilon$ is the differential photon density.

In our analysis one will follow C. D. Dermer and Menon 2009 to set up the pion resonance timescale. σ_{pr}, or the cross-section for the interaction is given by a two step function, and is given as

$$\sigma(E) = \begin{cases} 340\mu b, \mathrm{cm}^{-2} & \text{if } 390 m_e c^2 < E < 980 m_e c^2 \\ 120\mu b\, \mathrm{cm}^{-2} & \text{if } E > 980 m_e c^2 \end{cases} \tag{49}$$

addionally the inelasticity of the interaction, or how much energy is lost per interaction, is given as

$$K(E) = \begin{cases} 0.2 & \text{if } 390 m_e c^2 < E < 980 m_e c^2 \\ 0.6 & \text{if } E > 980 m_e c^2 \end{cases} \tag{50}$$

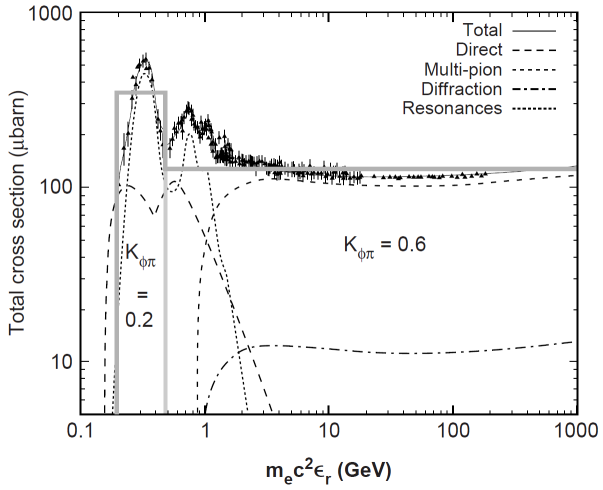

Figure 7: Pion resonance cross section, and the inelasticity of the interaction. Image taken from C. D. Dermer and Menon 2009

A Schematic view of the pion resonance cross-section and the inelasticity of the interaction is shown in figure 7.

The last important parameter in the pion production timescale is the photon field, and one will be using a photon field as described in section 4.2.3. The specific photon fields will be determined by what source one is looking at and will be clarified in due time.

5 Active Galactic Nuclei

1. Introduction to AGN
2. Why AGN serves as good candidates for UHECRs and neutrinos
3. The structure of AGNs
   (a) The central engine
   (b) The accretion disk
   (c) The corona
   (d) The torus
   (e) The broad-line region
   (f) The narrow-line region
   (g) The jet
   (h) The host galaxy
   (i) Types of outflows and particle leakadge
4. The different types of AGN
   (a) More boradly on the different types of AGN
   (b) Compact symmetric objects
   (c) Seyfert galaxies
   (d) Blazar types

6 Compact symmetric objects

1. Introduction to CSOs
2. What is a CSO
3. more on the structure of CSOs
4. The different types of CSOs
5. The prevalence of CSOs
6. CSO as candidates for UHECRs and neutrinos
   (a) Hillas criterion, Flux of X-ray compared to diffuse flux of UHECRs and neutrinos
   (b) Kinetic jet power
   (c) Timescale analysis

Introduction to CSOs

In regards to other types of AGN CSO or Compact symmetric objects are similar to Seyfert Galaxies. They are characterized by their small projected size which in Kiehlmann et al. 2023 is described by being less than one kiloparsec and having symmetric radio emissions on both sides of the central activity. They are also in the group of Jetted AGN, but are distinguish from other sources of jetted AGN because the jet is non-relativistic, and there is a lack of relativistic boosting. In the paper and subsequent papers by Kiehlmann et al. 2023 and their group there were some overlap in classification of some sources, were some sources were classified as CSOs when in relaity they were not. This was due to the fact that one overlooked two "new" properties of AGN that will also be important in this paper. CSOs are also characterized by low variability in radio and low apparent speed along the jet.

6.1 Structure of CSOs

This section will try to constate the structure of CSOs.

Total energy density

The total energy density of the photon fields as a function of distance is then seen in figure 8. Here one can see that the energy density of the photon fields is constant until the observer is outside the size of the respective regions. From the image it is clear that the biggest contributor to the total energy density becomes the IR torus, but all the regions contribute significantly to the total energy density.

Spectral energy density

The spectral energy density of the different regions is of more interest since this is what will determine the effect of pion decay on protons accelerate in the jet or in the lobes. To create the SED one has estimated the dynamical scale of our system and used the total photon densities to scale the SED accordingly. The resulting SED is seen in figure 9. The SED are determined also on a number of parameters, all which have taken from the literature. They are seen in table 1.

Parameter	Value
L_d	10^{43} erg/s
GM	$G10^8 M_\odot$
RS	$\frac{2GM}{c^2}$
η	0.1
f_X	0.3
R_X	$30RS$
β	0.4 c
$f_{\rm BLR}$	0.1
$R_{\rm BLR}$	$10^{17}\sqrt{L_d/10^{45}}$ cm
$f_{\rm IR}$	0.5
$R_{\rm IR}$	$2.5 10^{18}\sqrt{L_d/10^{45}}$ cm
Γ	1.1

Table 1: Parameters used to determine the SED of the different regions.

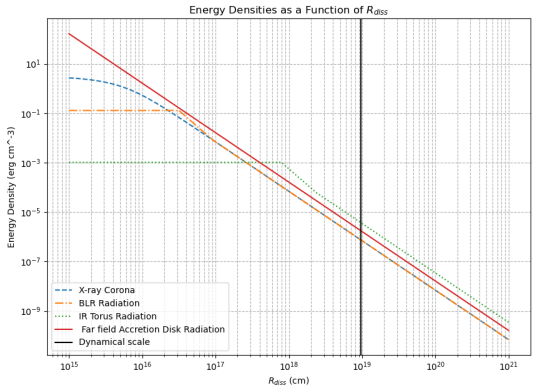

Figure 8: The total energy density of the photon fields as a function radius from central engine.

The choice of variables comes from three sources. Bronzini et al. 2024 and Kiehlmann et al. 2023 which both gives the disk luminosity of CSOs sources, and which we set to $10^{43} erg/s$. Ghisellini and Tavecchio 2009 gives the rest of parameters that relate the different regions to the disk luminosity. The biggest caveat here is that these parameters are not specific to CSOs, but to Blazars in which they are based. For the purposes of this analysis one assumes that the parameters are the same for CSOs as for Blazars, and that one would not expect any significant difference.

6.2 Classification of CSO

From the papers of Kiehlmann et al. 2023 to Readhead et al. 2023, and from Sullivan et al. 2024 there is a clear quite new classification of CSOs. The classification is based on firstly CSOs being edge brightened or edge dimmed. Edge brightened sources which will onwards be refered as CSO 2s are bright in radio in their lobes, and CSO 1s or edge dimmed are thought to be CSOs that have stalled.

The big picture on CSOs is that they are a group of very short-lived sources that are ignited by transient events. Saying if the ignition of their jets are due to transient event such as tidal disruption event are covered in Sullivan et al. 2024 and for the purposes of this study not necessary to discuss, but start a very interesting conversation. CSOs are then symmetric with the expansion of their jets into the interstellar medium visible from radio telescope. The symmetry of the jets is a key feature of CSOs and makes them unique in the sense

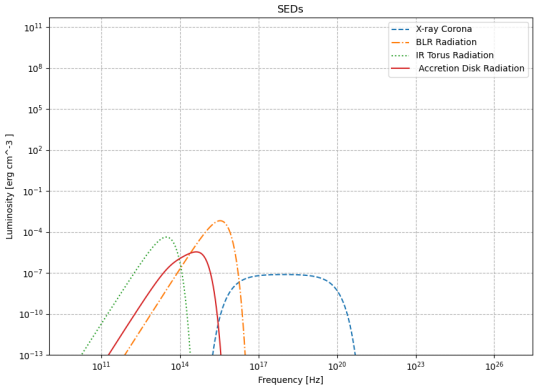

Figure 9: The spectral energy density at distance R

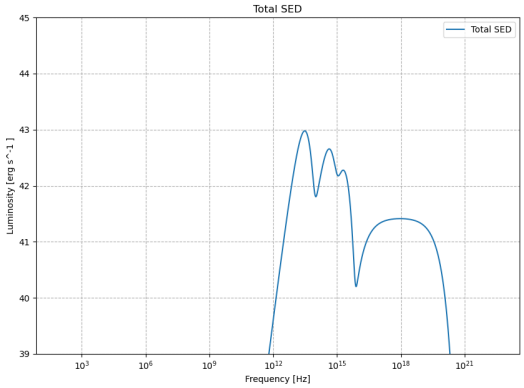

Figure 10: Luminosity of the different components of the CSO that are close by the central engine. Missing synchrotron and IC part which is most prominent

of jetted-AGN since they have little to no features of relativistic beaming.

6.3 Catalouge of Bona fide CSO

In order to study these sources there will always be a need for observational data. This fact combined with the fact that CSOs are a somewhat new class of AGN mean that there are no large catalogues of pure CSOs, and that many other catalogues misnomer sources as CSOs. This chapter will rely heavilly on Kiehlmann et al. 2023 in which this is discussed and where they define a bona fide catalogue of 79 CSOs. The catalogue will allow us as it has in this paper to say more concrete infromation about the sources we are studying.

6.4 Prevalence of CSOs

6.5 Stability in jet expansion and lobes.

The most promesing feature of CSOs which we will see as a key feature in the section on time-scales is the stability of the lobes in radio emission, the stability of the jet expansion and the stability of most wavelengths in emissions. In Bronzini et al. 2024 they report no significant variablilty of one CSO source in gamma rays, variability of the order of years in x-ray, with the broadband SED showing variability on the timescales of years. This is a clear distincsion from other jetted AGN which are known to be highly variable. Having stable systems allows for more efficient acceleration of ions, and significantly increases the possibility of producing UHECRs.

7 CSO as sources of UHECRs and neutrinos

8 Discussion

References

Alves, E. P., J. Zrake, and F. Fiuza (Dec. 2018). "Efficient Nonthermal Particle Acceleration by the Kink Instability in Relativistic Jets". In: *Physical Review Letters* 121.24. ISSN: 1079-7114. DOI: 10.1103/physrevlett.121.245101. URL: http://dx.doi.org/10.1103/PhysRevLett.121.245101.

Alves Batista, Rafael et al. (June 2019). "Open Questions in Cosmic-Ray Research at Ultrahigh Energies". In: *Frontiers in Astronomy and Space Sciences* 6. ISSN: 2296-987X. DOI: 10.3389/fspas.2019.00023. URL: http://dx.doi.org/10.3389/fspas.2019.00023.

Balasubramaniam, K. et al. (Nov. 2021). "X-Ray Emission of the gamma-ray-loud Young Radio Galaxy NGC 3894". In: *The Astrophysical Journal* 922.1, p. 84. ISSN: 1538-4357. DOI: 10.3847/1538-4357/ac1ff5. URL: http://dx.doi.org/10.3847/1538-4357/ac1ff5.

Bennun, Alfred (June 2020). "High Energy Dimensioning the Quantum Space-Time of the Electron". In.

Bronzini, E. et al. (2024). *Investigating X-ray Emission in the GeV-emitting Compact Symmetric Objects PKS 1718-649 and TXS 1146+596*. arXiv: 2401.16479 [astro-ph.HE].

collaboration, The Pierre Auger (May 2013). "Bounds on the density of sources of ultra-high energy cosmic rays from the Pierre Auger Observatory". In: *Journal of Cosmology and Astroparticle Physics* 2013.05, p. 009. DOI: 10.1088/1475-7516/2013/05/009. URL: https://dx.doi.org/10.1088/1475-7516/2013/05/009.

Collinson, James S. et al. (Oct. 2016). "Reaching the peak of the quasar spectral energy distribution – II. Exploring the accretion disc, dusty torus and host galaxy". In: *Monthly Notices of the Royal Astronomical Society* 465.1, pp. 358–382. ISSN: 0035-8711. DOI: 10.1093/mnras/stw2666. eprint: https://academic.oup.com/mnras/article-pdf/465/1/358/8593036/stw2666.pdf. URL: https://doi.org/10.1093/mnras/stw2666.

Dermer, Charlees D. and Govind Menon (2009). *High Energy Radiation from Black Holes: Gamma Rays, Cosmic Rays, and Neutrinos*. Princeston University Press.

Dermer, Charles (Jan. 2001). "Maximum Particle Energies by Fermi Acceleration and the Origin of Cosmic Rays above the Knee". In.

Ghisellini, G. and F. Tavecchio (Aug. 2009). "Canonical high-power blazars". In: *Monthly Notices of the Royal Astronomical Society* 397.2, pp. 985–1002. ISSN: 1365-2966. DOI: 10.1111/j.1365-2966.2009.15007.x. URL: http://dx.doi.org/10.1111/j.1365-2966.2009.15007.x.

Hillas, A. M. (1984). "The Origin of Ultra-High-Energy Cosmic Rays". In: *Annual Review of Astronomy and Astrophysics* 22.1, pp. 425–444. DOI: 10.1146/annurev.aa.22.090184.002233. URL: https://doi.org/10.1146/annurev.aa.22.090184.002233.

Hirotani, Kouichi (Jan. 2005). "Kinetic Luminosity and Composition of Active Galactic Nuclei Jets". In: *The Astrophysical Journal* 619.1, pp. 73–85. ISSN: 1538-4357. DOI: 10.1086/426497. URL: http://dx.doi.org/10.1086/426497.

Hogg, David W. (2000). *Distance measures in cosmology*. arXiv: astro-ph/9905116 [astro-ph].

Kiehlmann, S. et al. (2023). *Compact Symmetric Objects – I Towards a Comprehensive Bona Fide Catalog*. arXiv: 2303.11357 [astro-ph.HE].

Marscher, A. P. (1983). "Accurate formula for the self-Compton X-ray flux density from a uniform, spherical, compact radio source." In: *apj* 264, pp. 296–297. DOI: 10.1086/160597.

O'Sullivan, S., B. Reville, and A. M. Taylor (Nov. 2009). "Stochastic particle acceleration in the lobes of giant radio galaxies". In: *Monthly Notices of the Royal Astronomical Society* 400.1, pp. 248–257. ISSN: 1365-2966. DOI: 10.1111/j.1365-2966.2009.15442.x. URL: http://dx.doi.org/10.1111/j.1365-2966.2009.15442.x.

Orienti, M. and D. Dallacasa (Dec. 2013). "Physical properties of young radio sources: VLBA observations of high-frequency peaking radio sources". In: *Monthly Notices of the Royal Astronomical Society* 438.1, pp. 463–475. ISSN: 0035-8711. DOI: 10.1093/mnras/stt2217. eprint: https://academic.oup.com/mnras/article-pdf/438/1/463/18463416/stt2217.pdf. URL: https://doi.org/10.1093/mnras/stt2217.

Readhead, A. C. S. et al. (2023). *Compact Symmetric Objects – III Evolution of the High-Luminosity Branch and a Possible Connection with Tidal Disruption Events*. arXiv: 2303.11361 [astro-ph.HE].

Sullivan, Andrew G. et al. (2024). *Small-scale radio jets and tidal disruption events: A theory of high-luminosity compact symmetric objects*. arXiv: 2401.14399 [astro-ph.HE].

Wilson, Thomas L., Kristen Rohlfs, and Susanne Huttemeister (2013). *Tools of Radio Astronomy*. DOI: 10.1007/978-3-642-39950-3.